Science Advances
AAAS

advances.sciencemag.org/cgi/content/full/5/5/eaav3660/DC1

Supplementary Materials for

Molecular mechanism and potential target indication of TAK-931, a novel CDC7-selective inhibitor

Kenichi Iwai, Tadahiro Nambu, Ryo Dairiki, Momoko Ohori, Jie Yu, Kristine Burke, Masamitsu Gotou, Yukiko Yamamoto, Shunsuke Ebara, Sachio Shibata, Ryosuke Hibino, Satoru Nishizawa, Tohru Miyazaki, Misaki Homma, Yuya Oguro, Takashi Imada, Nobuo Cho, Noriko Uchiyama, Akifumi Kogame, Toshiyuki Takeuchi, Osamu Kurasawa, Kazunori Yamanaka, Huifeng Niu, Akihiro Ohashi*

*Corresponding author. Email: aohashi@east.ncc.go.jp

Published 22 May 2019, *Sci. Adv.* **5**, eaav3660 (2019)
DOI: 10.1126/sciadv.aav3660

This PDF file includes:

A

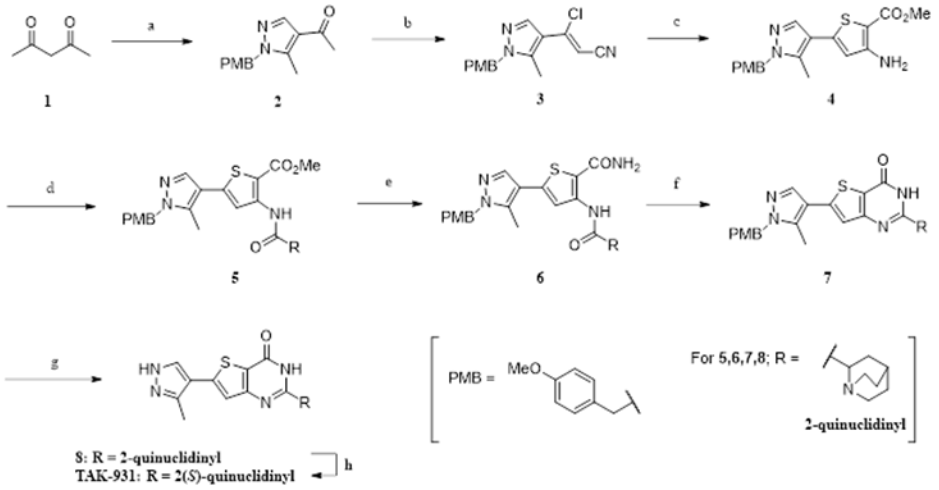

C

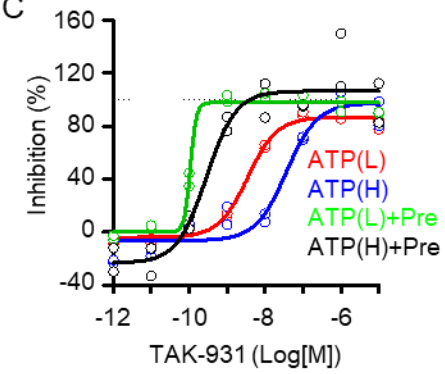

D

K_D	K_{off} (sec^{-1})	Residence Time (min)
$4.24X10^{-10}$	$6.30X10^{-4}$	26

B

Enzyme	IC_{50} (nM)	% inhibition at 1000nM
Cdc7/DBF4	<0.3	N/A
DAPK3 (ZIPK)	160	98.8
DAPK1	49.8	96.1
CDK9/cyclin T1	36.9	94.7
DMPK	44.2	94.1
CDK8/cyclin C	101	91.0
MAPK12 (p38 gamma)	155	85.1
STK17A (DRAK1)	115	84.4
CLK4	99.0	84.1
DYRK1A	148	82.0
GSK3B (GSK3 beta)	338	80.5
307 kinase assays	N.T.	< 80

E

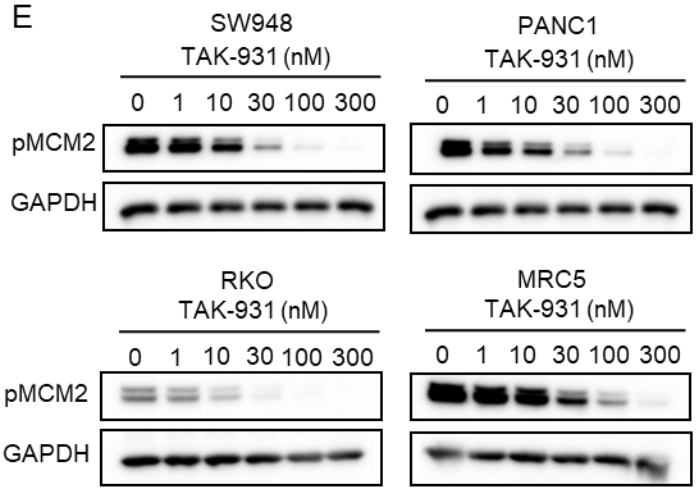

F

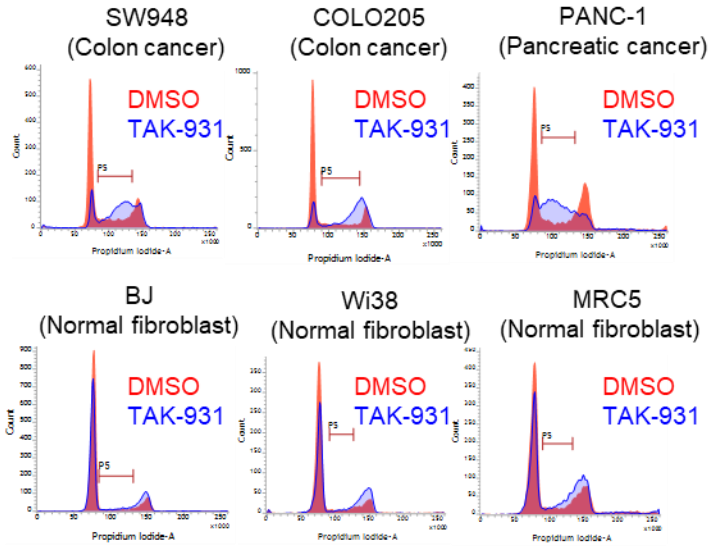

G

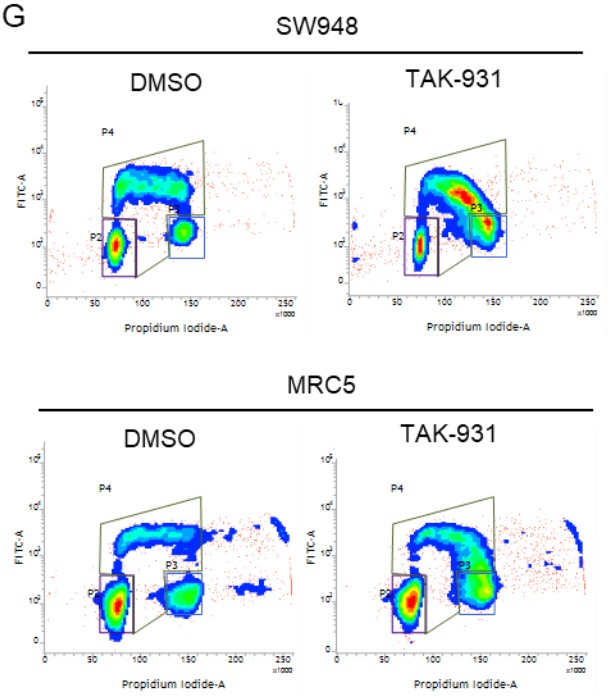

Fig. S1. In vitro pharmacological profile of TAK-931. (A) Reagents and conditions: (a) **1**, *N*,*N*-dimethylformamide dimethyl acetal, 80 °C, 1 h, then EtOH, Et_3N, *p*-methoxybenzyl(PMB)-hydrazine hydrochloride, 0 °C to room temperature, overnight; (b) DMF, $POCl_3$, 0 °C, 15 min, then **2**, 0 °C to 60 °C, 30 min, then hydroxylamine hydrochloride, 80 °C, 30 min; (c) methyl thioglycolate, NaH, DMF, 0 °C, 5 min, then **3**, 40 °C, 2 h; (d) 2-quinuclidinecarboxylic acid, $SOCl_2$, 30 °C, 18 h, then **4**, DIEA, THF, room temperature to 60 °C, 75 min; (e) **5**, NaOH, MeOH, 60 °C, 1.5 h, then EDCI, HOBt, Et_3N, NH_4Cl, DMF, room temperature overnight; (f) **6**, NaOH, EtOH, 70 °C, 2 h; (g) **7**, TFA, anisole, 90 °C, 18 h; (h) **8**, Preparative HPLC (CHIRALPAK AD). (B) TAK-931 exhibits high-selectivity toward CDC7 kinase. The 318 kinases were used for enzymatic assay. The IC_{50} values and % inhibition at 1,000 nM of TAK-931 are shown. (C) TAK-931 is an ATP-competitive CDC7 inhibitor with slow-binding kinetics. The red and blue lines indicate low (1 μM) and high (50 μM) ATP concentrations in the absence of preincubation (-), respectively. The green and black lines indicate low and high ATP concentrations in the presence of preincubation (+), respectively. (D) K_D values of TAK-931. Kinetics analysis for TAK-931 was performed by surface plasmon resonance (SPR) in the Proteros reporter displacement assay. (E) Cellular activity of TAK-931. SW948, PANC-1, RKO, and MRC5 cells were treated with the indicated concentration of TAK-931 for 4 h. pMCM2 was used for the target engagement markers of CDC7 kinase. GAPDH was used for the loading controls. (F) Effect of TAK-931 on stalled S phase between cancer cell lines and untransformed fibroblasts. COLO205, SW948, and PANC-1 were used as representative cancer cell lines. BJ, WI38, and MRC5 were used as representative untransformed fibroblasts. The cells were treated with DMSO (control, red) and TAK-931 (300 nM, blue). The cells were collected 24 h after TAK-931 treatment and analyzed by flow cytometry. (G) Effect of

TAK-931 on BrdU incorporation in SW948 and MRC5 cells. The cells were treated with DMSO (red) or TAK-931 (300 nM, blue) for 24 h, and then BrdU was incorporated for 30 min. The cells were stained with PI and anti-BrdU antibody to be analyzed by flow cytometry.

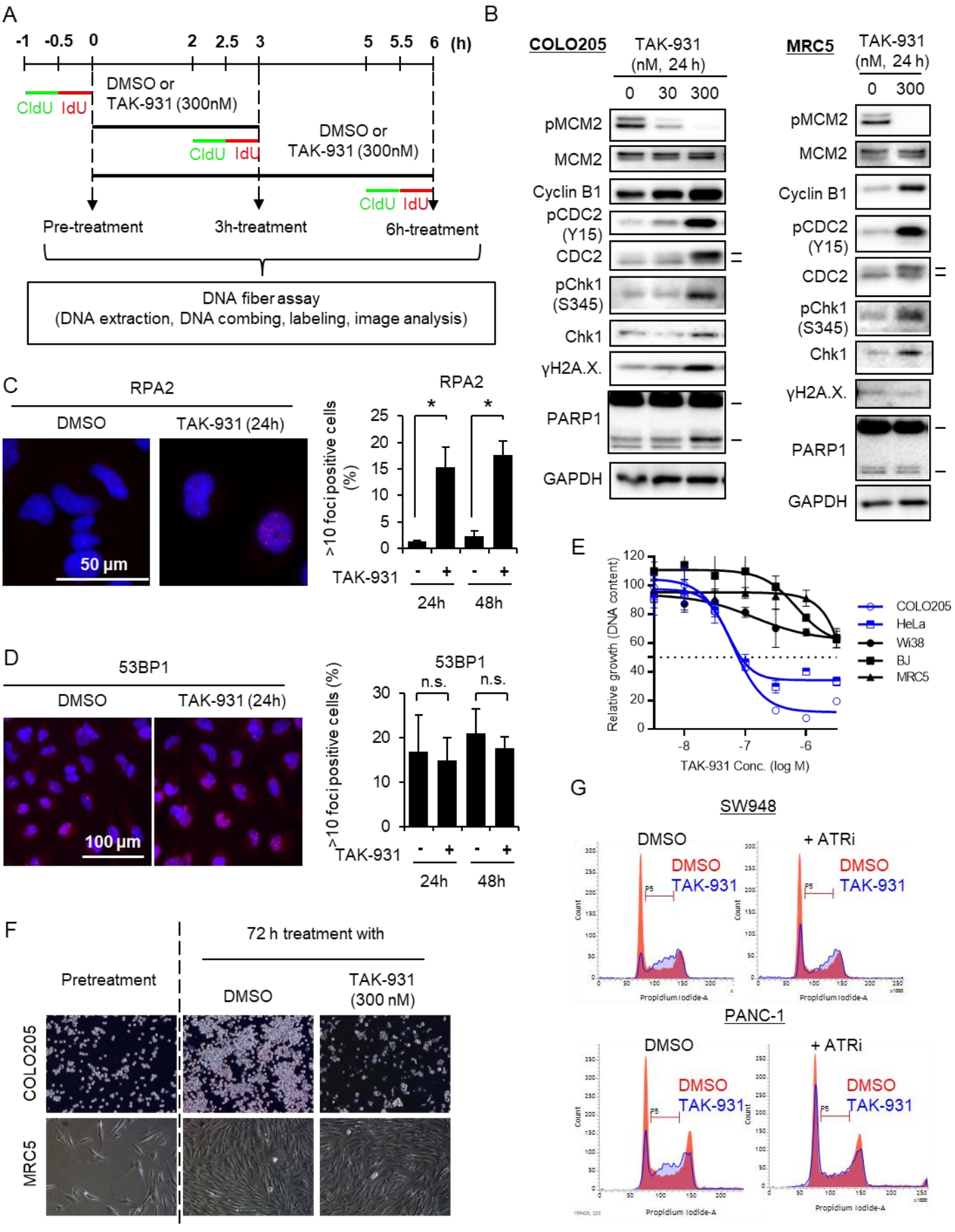
A
-1 -0.5 0 2 2.5 3 5 5.5 6 (h)
CldU IdU
DMSO or TAK-931 (300nM)
CldU IdU
DMSO or TAK-931 (300nM)
CldU IdU
Pre-treatment
3h-treatment
6h-treatment
DNA fiber assay
(DNA extraction, DNA combing, labeling, image analysis)
B
COLO205
TAK-931 (nM, 24 h)
0 30 300
pMCM2
MCM2
Cyclin B1
pCDC2 (Y15)
CDC2
pChk1 (S345)
Chk1
γH2A.X.
PARP1
GAPDH
MRC5
TAK-931 (nM, 24 h)
0 300
pMCM2
MCM2
Cyclin B1
pCDC2 (Y15)
CDC2
pChk1 (S345)
Chk1
γH2A.X.
PARP1
GAPDH
C
RPA2
DMSO
TAK-931 (24h)
50 μm
RPA2
>10 foci positive cells (%)
TAK-931
24h
48h
D
53BP1
DMSO
TAK-931 (24h)
100 μm
53BP1
n.s.
>10 foci positive cells (%)
TAK-931
24h
48h
E
Relative growth (DNA content)
TAK-931 Conc. (log M)
COLO205
HeLa
Wi38
BJ
MRC5
F
72 h treatment with
Pretreatment
DMSO
TAK-931 (300 nM)
COLO205
MRC5
G
SW948
DMSO
+ ATRi
DMSO
TAK-931
Propidium Iodide-A
PANC-1
DMSO
+ ATRi
DMSO
TAK-931
Propidium Iodide-A

Fig. S2. Effect of TAK-931 on DNA replication, RS, and DDR. (A) Experimental schemes for DNA fiber assay. HeLa cells were treated with DMSO or TAK-931 (300 nM) for the indicated periods. The cells were sequentially incubated with CldU (green) and IdU (red) for 30 min for each. After CldU/IdU incorporation, the cells were collected for DNA fiber assay according to the manufacturer's procedures (GenomicVision). (B) Effects of TAK-931 on DDR, DNA damage checkpoint, and apoptosis in COLO205 (left) and MRC5 (right). The cells were treated with TAK-931 at the indicated concentrations for 24 h. Immunoblotting for pMCM2, MCM2, cyclin B1, pCDC2, pCHK1, CHK1, γH2A.X, PARP1, and GAPDH was performed. Upper band of CDC2 indicates phosphorylated CDC2. Lower band of PARP1 indicates cleaved PARP1. MCM2 and GAPDH were used for loading controls. (C) (D) Effect of TAK-931 on RPA2 and 53BP1 foci formation. HeLa cells were treated with DMSO or TAK-931 (300 nM) for 24 h. Immunofluorescence for RPA2 (C) and 53BP1 (D) was performed. PRA2 and 53BP1 were used as markers for SSBs and DSBs, respectively. Red signals indicate PRA2 (C) or 53BP1 (D). Blue signals indicate DAPI (DNA). White bars indicate 50 μm (left) or 100 μm (right). Y-axis indicate % cells with >10 foci per nucleus. Data are presented as the mean ± SD (n = 3). Differences were considered significant at $p \leq 0.05$ (*). (E) Effect of TAK-931 on antiproliferation in cancer cells (COLO205 and HeLa) and untransformed fibroblasts (WI38, BJ, and MRC5). The cells were treated with TAK-931 at the indicated concentrations for 72 h (n=3). Relative DNA contents were calculated relative to the DNA content of 0 nM TAK-931 treatment. (F) Representative pictures of COLO205 and MRC5 with or without TAK-931 treatment (300 nM, 72 h). (G) Effect of ATR on TAK-931-induced DNA replication stalling in SW948 (upper) and PANC-1 (lower). The cells were treated with DMSO (red, left), TAK-931

(300 nM, blue at left), ATR inhibitor (VE-821, 1 μM, red at right), and combination (blue, right). The cells were collected 24 h after TAK-931 treatment and analyzed by flow cytometry.

A

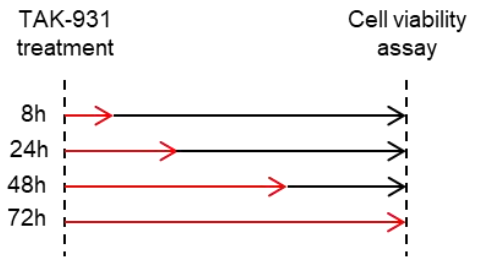

B

Phosphorylation Status	Numbers
Quantified phosphorylation sites (class I, localization probability ≥ 0.75)	15,128 Ser (P): 85%, Thr (P): 14%, Tyr (P): 1%
Quantified phosphoproteins	4, 426
Regulated phosphorylation sites	52 in total (4h: 2 sites, 24h: 51 sites,1 site overlapped)
Regulated phosphoproteins	43

C

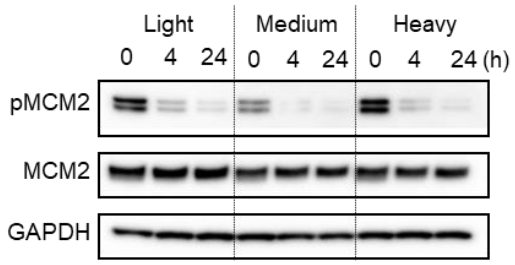

D

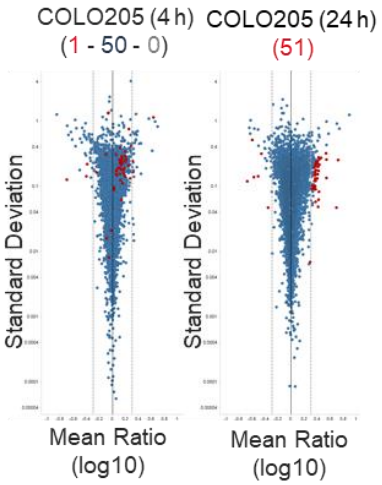

E

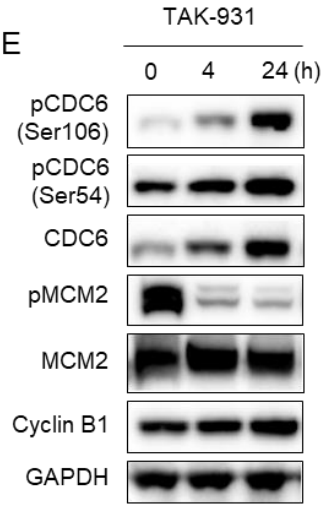

F

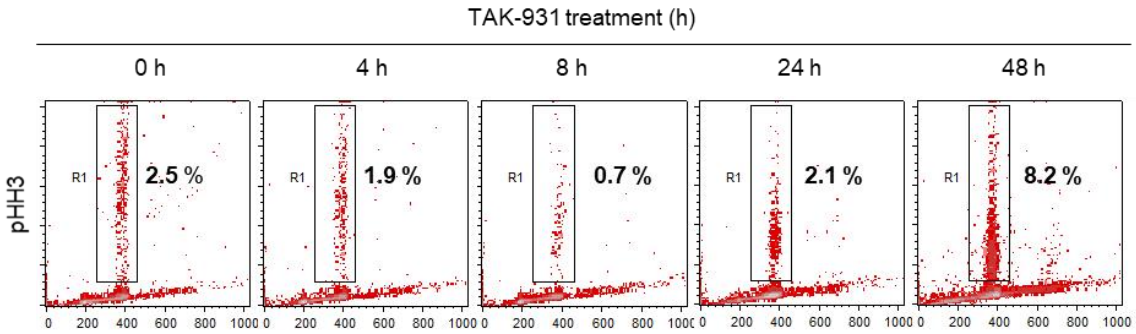

G

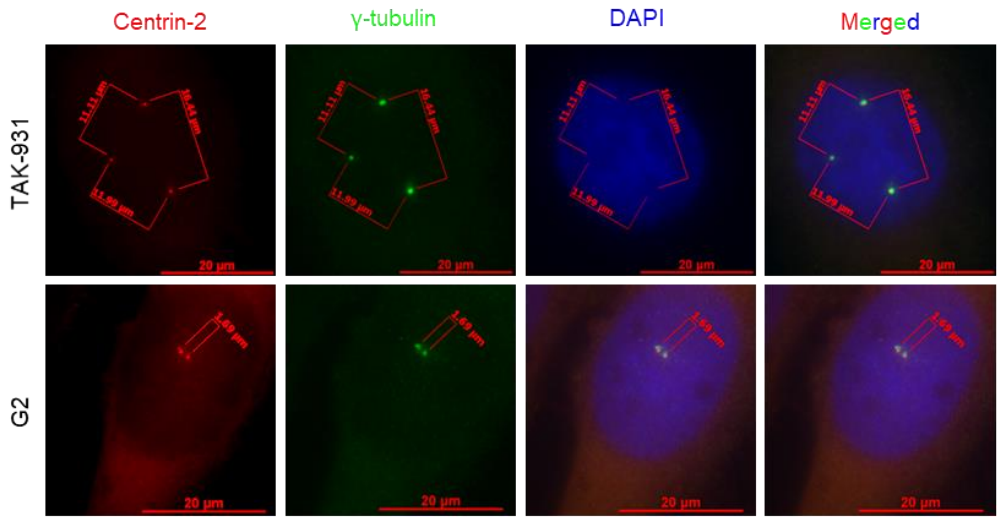

Fig. S3. Irreversible antiproliferative effects of TAK-931 and mitotic aberrations. (A) Experimental schemes to assess time-dependent antiproliferative activity of TAK-931. COLO205 cells were treated with TAK-931 at the indicated concentrations for 8, 24, 48, and 72 h (red arrows) and then cultured in TAK-931−free medium (black arrows). Cells were collected 72 h after treatment for cell viability analysis. (B) Summary of phosphorylation detected by phosphoproteomics analysis. (C) Immunoblotting analysis in SILAC-labeled COLO205 cells. COLO205 cells cultured in light, medium, or heavy SILAC media were treated with TAK-931 at 100 nM for 0, 4, or 24 h, then immunoblotting of pMCM2, MCM2, and GAPDH was performed; MCM2 and GAPDH were used as loading controls. (D) Volcano plot of quantified phosphorylation sites. The x-axis indicates the $\log_{10}$-scaled mean ratio of each phosphorylation site between TAK-931 and DMSO treatments. Plus and minus indicate upregulation and downregulation, respectively; dotted lines indicate 2-fold changes. The y-axis indicates the standard deviation. The volcano plots of 4 h (left) and 24 h (right) treatments are shown. The significantly changed phosphorylation sites at 24 h treatment are depicted in red. (E) Immunoblotting forpCDC6 (Ser-106, Ser-54), CDC6, cyclin B1, pMCM2 (Ser-40), MCM2, and GAPDH was performed. MCM2 and GAPDH were used for loading controls. COLO205 cells were treated with TAK-931 at 100 nM for 24 h. (F) Effect of TAK-931 on mitotic arrest in a time-dependent manner. HeLa cells were treated with TAK-931 at 300 nM for the indicated number of hours. pHH3 was used as a mitotic index. R1 indicates the % pHH3-positive cells. (G) Representative immunofluorescence images of centrosomal markers. Upper and lower images depict TAK-931-treated and G2 synchronous HeLa cells, respectively. Red: centrin-2, green: γ-tubulin, and blue: DAPI. The distances between centrosomes were measured by AxioVision.

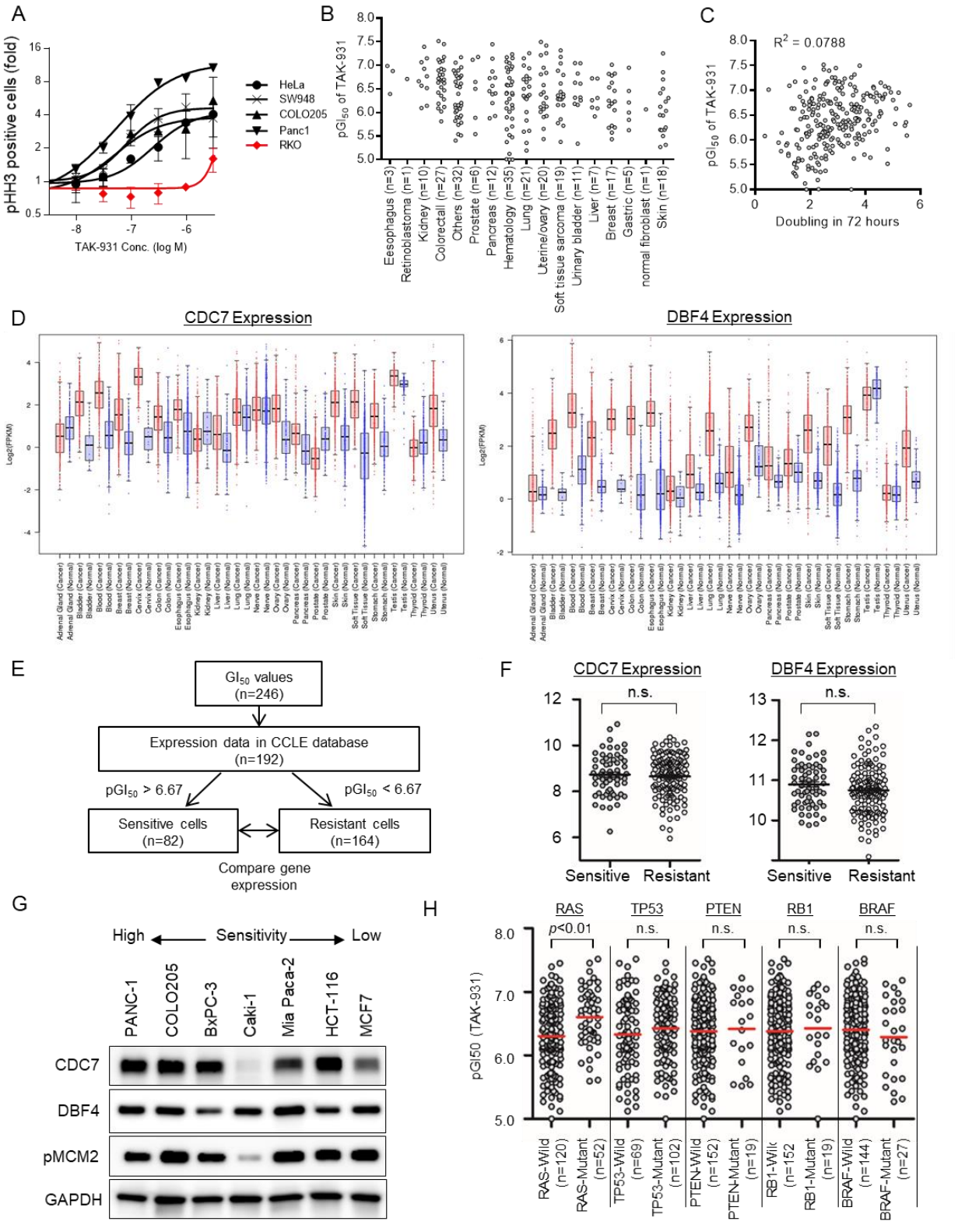
A
pHH3 positive cells (fold)
TAK-931 Conc. (log M)
HeLa
SW948
COLO205
Panc1
RKO
B
pGI50 of TAK-931
Eesophagus (n=3)
Retinoblastoma (n=1)
Kidney (n=10)
Colorectall (n=27)
Others (n=32)
Prostate (n=6)
Pancreas (n=12)
Hematology (n=35)
Lung (n=21)
Uterine/ovary (n=20)
Soft tissue sarcoma (n=19)
Urinary bladder (n=11)
Liver (n=7)
Breast (n=17)
Gastric (n=5)
normal fibroblast (n=1)
Skin (n=18)
C
R2 = 0.0788
pGI50 of TAK-931
Doubling in 72 hours
D
CDC7 Expression
DBF4 Expression
Log2(FPKM)
E
GI50 values (n=246)
Expression data in CCLE database (n=192)
pGI50 > 6.67
pGI50 < 6.67
Sensitive cells (n=82)
Resistant cells (n=164)
Compare gene expression
F
CDC7 Expression
DBF4 Expression
n.s.
Sensitive
Resistant
G
High
Sensitivity
Low
PANC-1
COLO205
BxPC-3
Caki-1
Mia Paca-2
HCT-116
MCF7
CDC7
DBF4
pMCM2
GAPDH
H
RAS
TP53
PTEN
RB1
BRAF
p<0.01
n.s.
pGI50 (TAK-931)
RAS-Wild (n=120)
RAS-Mutant (n=52)
TP53-Wild (n=69)
TP53-Mutant (n=102)
PTEN-Wild (n=152)
PTEN-Mutant (n=19)
RB1-Wild (n=152)
RB1-Mutant (n=19)
BRAF-Wild (n=144)
BRAF-Mutant (n=27)

Fig. S4. Large-scale in vitro cell panel studies of TAK-931. (A) Fold increase curves of pHH3-positive cells by TAK-931 in the representative cancer cell lines are shown (HeLa, SW948, COLO205, PANC-1, and RKO cells). Cells were stained with fluorescently-labeled pHH3 antibody 72 h after TAK-931 treatment at the indicated concentrations. The fold-change in pHH3-positive cells was calculated relative to % pHH3 positive cells with 0 nM TAK-931 treatment. (B) GI_{50} values of TAK-931 in each pathological type of the 246 cancer cell lines. (C) No significant correlation was observed between TAK-931 sensitivity and the doubling-speed in the 246 cancer cell lines. (D) Expression of CDC7 and DBF4 in normal and cancer tissues. The mRNA expressions of CDC7 (left) and DBF4 (right) in normal and cancer tissues are shown. The databases of Genotype-Tissue Expression (GTEX, normal tissue), International Cancer Genome Consortium (ICGC, cancer tissue), and the Cancer Genome Atlas (TCGA, cancer tissue) were used. Red and blue indicate cancer and normal tissues, respectively. (E) Experimental schemes to evaluate the correlation between TAK-931 sensitivity and CDC7/DBF4 expression. The expression data in the Cancer Cell Line Encyclopedia (CCLE) database were used. A total of 192 of 246 cell lines, for which expression data were available in the CCLE database, were divided into sensitive ($pGI_{50} > 6.67$) and resistant ($pGI_{50} < 6.67$) cell line groups, and the expression levels of CDC7/DBF4 were compared. (F) Correlation of TAK-931 with CDC7/DBF4 expression. Dot plots of CDC7 (left) or DBF4 (right) expression values between TAK-931-sensitive ($pGI_{50}>6.67$, n=82) and TAK-931-resistant ($pGI_{50}<6.67$, n=164) cell lines are shown. The red lines indicate mean pGI_{50} values in each group. Statistical analyses were performed using Student's *t*-tests. Differences were considered significant at $p<0.05$. n.s., not significant. (G) Effect of baseline expression of CDC7, DBF4, and pMCM2 between sensitive and insensitive cancer cell lines. Seven cancer cell lines were used to evaluate the baseline

expression of CDC7, DBF4, and pMCM2. GAPDH was used for loading controls. (H) Dot plots of TAK-931 GI_{50} values in mutant and wildtype cell lines with RAS, TP53, PTEN, RB1, and BRAF mutations. Red lines indicate mean pGI50 values in each group. Sequence data in the CCLE database were used. Statistical analysis was performed using Student's t-tests.

A

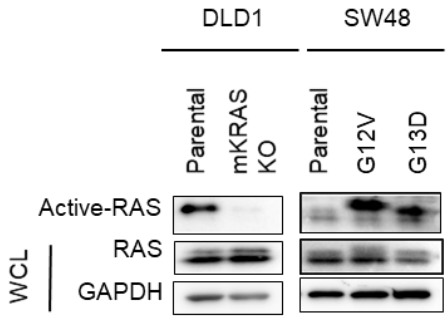

B

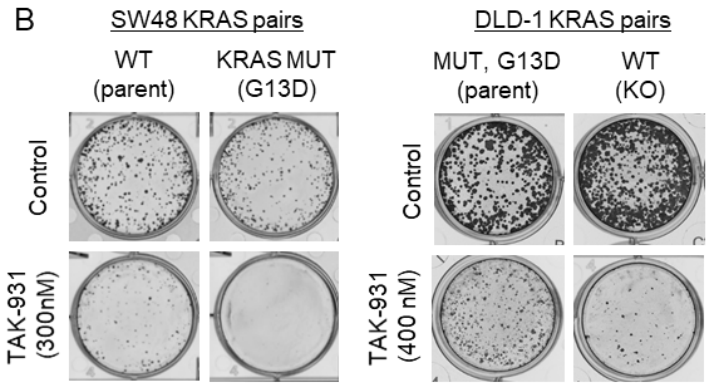

C

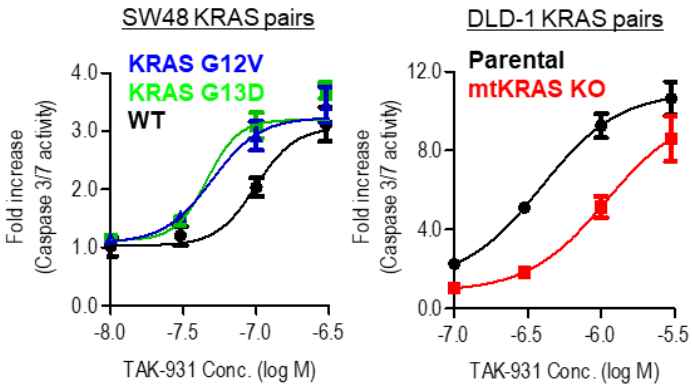

D

Drugs	Mechanism	Cell Line Numbers	Median IC50 Values ±SEM
Cisplatin	platinum compound	228	4.92 ± 0.03
Carboplatin	platinum compound	206	4.51 ± 0.05
Oxaliplatin	platinum compound	232	5.78 ± 0.04
Gemcitabine	antimetabolite	224	7.90 ± 0.03
Methotrexate	antimetabolite	156	7.45 ± 0.04
SN-38	topoisomerase inhibitor	228	8.42 ± 0.05
Doxorubicin	topoisomerase inhibitor	203	7.45 ± 0.04
Paclitaxel	tubulin binder	187	8.49 ± 0.04

E

	TAK-931	Doxorubicin	Oxaliplatin	SN-38	Carboplatin	Paclitaxel	Cisplatin	Gemcitabine	Methotrexate
TAK-931	-	0.51	0.47	0.36	0.35	0.33	0.32	0.29	0.28
Doxorubicin	0.51	-	0.56	0.53	0.45	0.65	0.50	0.36	0.37
Oxaliplatin	0.47	0.56	-	0.45	0.46	0.33	0.46	0.22	0.41
SN-38	0.36	0.53	0.45	-	0.41	0.35	0.41	0.28	0.38
Carboplatin	0.35	0.45	0.46	0.41	-	0.21	0.72	0.34	0.30
Paclitaxel	0.33	0.65	0.33	0.35	0.21	-	0.28	0.13	0.15
Cisplatin	0.32	0.50	0.46	0.41	0.72	0.28	-	0.45	0.37
Gemcitabine	0.29	0.36	0.22	0.28	0.34	0.13	0.45	-	0.20
Methotrexate	0.28	0.37	0.41	0.38	0.30	0.15	0.37	0.20	-

F

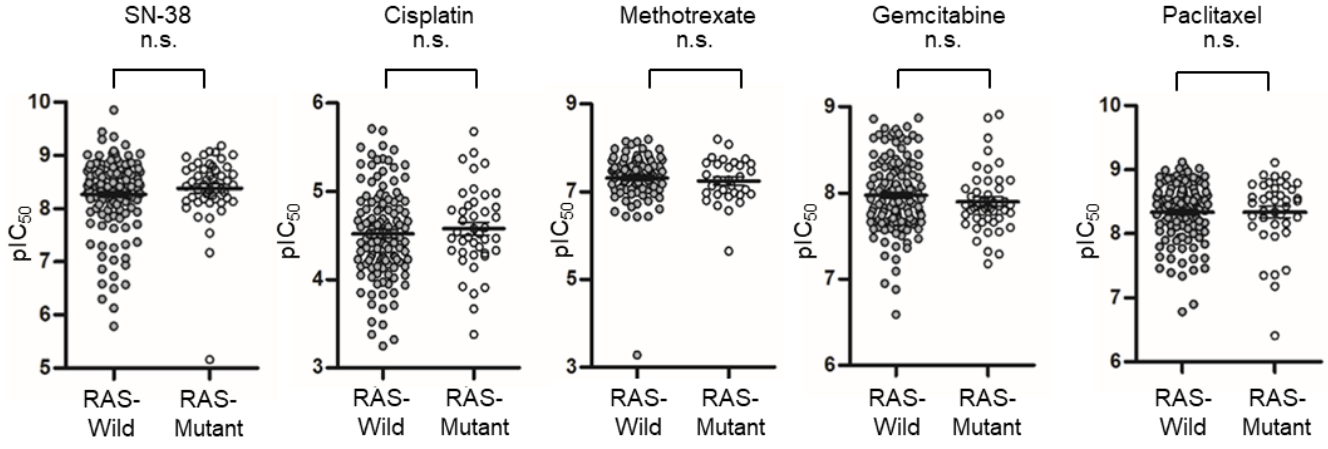

Fig. S5. Effect of KRAS mutation on TAK-931 antiproliferative activity, showing unique antiproliferative spectrum in cancer cells. (A) Active RAS was significantly increased in both DLD1-based and SW48-based isogenic cell lines of KRAS mutations. Active RAS was pulled down by GST-fusion protein of the Ras-binding domain (RBD) of Raf1, and then detected by immunoblotting with anti-RAS antibody. RAS and GAPDH in whole cell lysate (WCL) were used for loading controls. (B) Colony formation assays in *KRAS*-mutant or *KRAS*-wildtype cells with or without TAK-931 treatment. SW48-bsaed (left) and DLD1-based (right) isogenic cell line pairs were sued. Representative images of crystal violet staining are shown. (C) Effect of *KRAS* mutation on caspase-3/7 induction by TAK-931 treatment. SW48-based (left) and DLD1-based (right) isogenic cell line pairs were treated with TAK-931 at the indicated concentrations for 24 h. Fold increases in caspase-3/7 activity were calculated with chemiluminescence assay and compared with the chemiluminescence value of 0 nM TAK-931 treatment in each cell. (D) Summary of GI_{50} values of the following chemotherapeutic drugs in various cancer cell lines: cisplatin, carboplatin, oxaliplatin, gemcitabine, methotrexate, SN-38, doxorubicin, and paclitaxel. (E) Summary of correlation coefficient (R) of the GI_{50} values of TAK-931 and the GI_{50} values of the indicated chemotherapeutic drugs. Red, yellow, and green indicate $R > 0.7$, $0.7 \geq R > 0.4$, and $R \leq 0.4$, respectively. (F) Dot plots of GI50 values in *RAS*-mutant and -wildtype cell lines for SN-38, carboplatin, doxorubicin, gemcitabine, and paclitaxel. Sequence data in the CCLE database were used. Statistical analyses were performed using Student's t-tests for cisplatin, and the Wilcoxon-Mann-Whitney test for SN-38, methotrexate, gemcitabine, and paclitaxel.

A

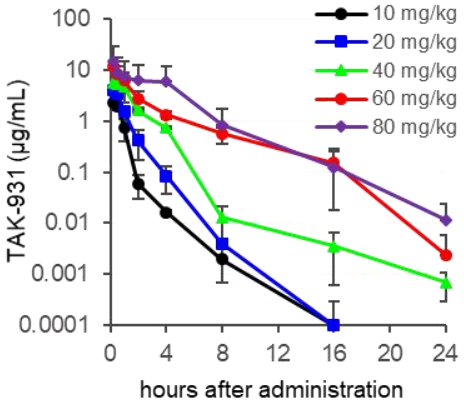

B

Dose	Plasma				Tumor			
	Tmax	Cmax	MRT	AUC_{0-72h}	Tmax	Cmax	MRT	AUC_{0-72h}
(mg/kg)	(h)	(μg/mL)	(h)	(μg·h/mL)	(h)	(μg/g)	(h)	(μg·h/g)
10	0.25	2.3383	0.77	2.0293	0.25	1.3771	1.79	2.0119
20	0.25	4.0097	1.04	4.2747	0.50	2.2451	2.30	4.3140
40	0.25	5.6971	1.76	11.6569	0.50	3.9779	3.72	10.6385
60	0.25	11.3771	3.34	23.2798	0.50	5.3187	4.00	18.4444
80	0.25	14.6468	3.47	45.3914	4.00	5.1722	6.86	44.3332

C

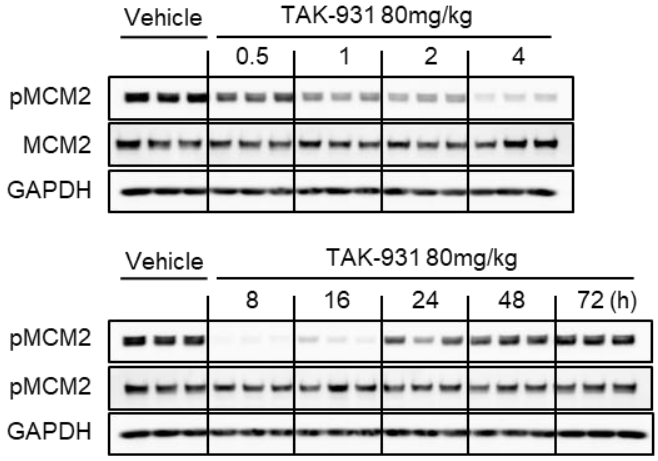

D

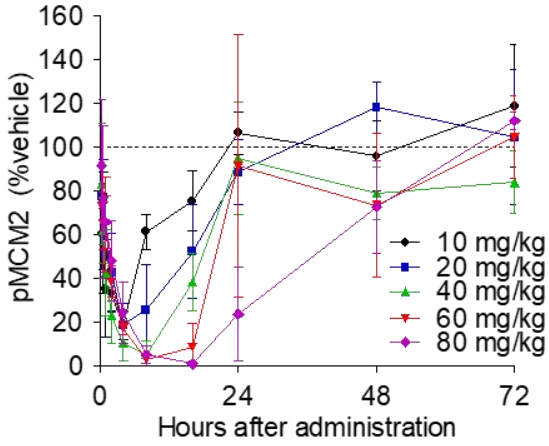

E

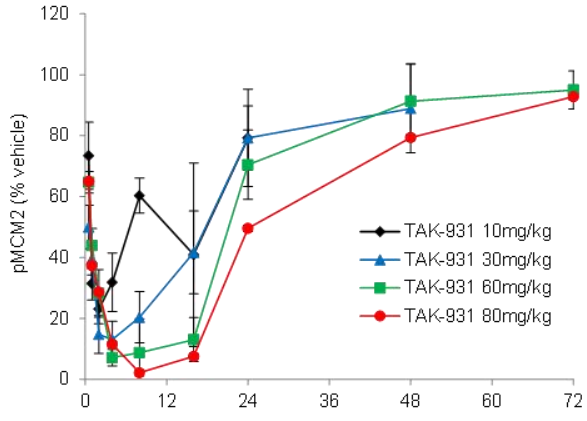

F

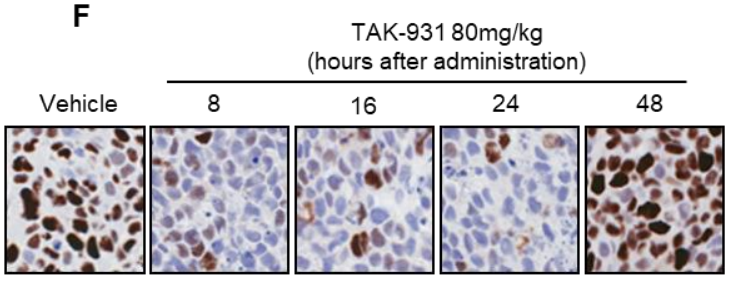

G

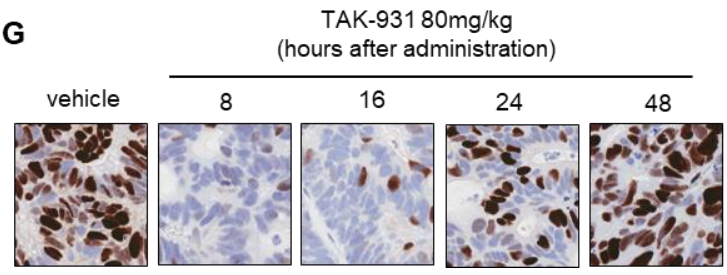

Fig. S6. PK/PD/efficacy study of TAK-931 in tumor xenograft mouse model. (A) Time- and dose-dependent plasma PK of TAK-931. Plasma was collected to measure drug concentrations at the indicated time points after TAK-931 oral administration. Black, blue, green, red, and purple lines indicate 10, 20, 40, 60, and 80 mg/kg doses. (B) Summary of TAK-931 PK profile in plasma and tumor. COLO205-xenografted nude mice were orally administered TAK-931 at the indicated doses. Time at peak serum concentration (T_{max}), peak serum concentration (C_{max}), mean resident time (MRT), and area under the curve from 0–72 h ($AUC_{0\text{-}72h}$) are shown. (C) Expression of pMCM2 in SW948 xenografts at the indicated time points after oral administration of TAK-931 at a dose of 80 mg/kg. MCM2 and GAPDH were used as controls. (D) Time- and dose-dependent PD of TAK-931 in COLO205 xenografts. COLO205 xenografts were collected to measure pMCM2 expression at the indicated time points after TAK-931 oral administration. Black, blue, green, orange, and red lines indicate 10, 20, 40, 60, and 80 mg/kg doses. The pHH3 intensity was quantified using immunoblotting, and normalized to the intensity of vehicle control. (E) Time- and dose-dependent PD of TAK-931. SW948 xenografts were collected to measure pMCM2 expression at the indicated time points after TAK-931 oral administration. Black, blue, green, and red lines indicate 10, 30, 60, and 80 mg/kg doses, respectively. pHH3 intensity was quantified using immunoblotting, and normalized to the intensity of vehicle control. (F) (G) Immunohistochemistry of pMCM2 in the tumor sections from COLO205 (F) and SW948 (G) xenograft nude mice at the indicated time points after oral administration of TAK-931 at 80 mg/kg.

A

Regimen	T/C (%)	BWC (%)	Death
Vehicle	-	+5.6	0/5
10 mg/kg, bid	63	+2.2	0/5
20 mg/kg, bid	67	-0.5	0/5
40 mg/kg, bid	9	-0.1	0/5
60 mg/kg, bid	-17	-10.2	0/5

B

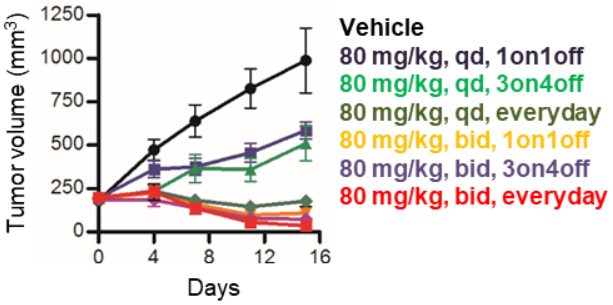

C

Regimen	T/C (%)	BWC (%)	Death
Vehicle	-	-2.6	0/5
80 mg/kg, qd,1 day on/1 day off	48	+4.7	0/5
80 mg/kg, qd, 3 day on/3 day off	39	+6.1	0/5
80 mg/kg, bid, 1 day on/1 day off	-11	+4.0	0/5
80 mg/kg, bid, 3 day on/4 day off	-14	+6.5	0/5
80 mg/kg, qd, Everyday	-3	-4.2	0/5
60 mg/kg, bid, Everyday	-20	-13.9	0/5

D

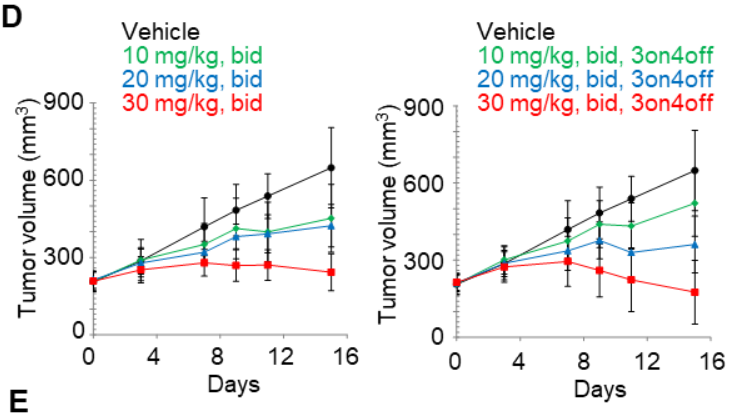

E

Regimen	T/C (%)	BWC (%)	Death
Vehicle	-	-11.5	0/8
10 mg/kg, bid, Day1-14	55	-13.6	0/8
20 mg/kg, bid, Day1-14	47	-18.6	0/8
30 mg/kg, bid, Day1-14	8	-15.2	1/8 (Day9)
20 mg/kg, bid, Day1-3, 8-10	71	-13.4	0/8
40 mg/kg, bid, Day1-3, 8-10	34	-12.9	0/8
60 mg/kg, bid, Day1-3, 8-10	-9	-11.6	0/8

F

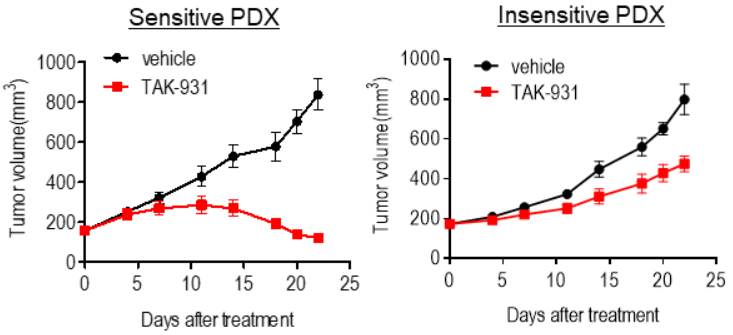

G

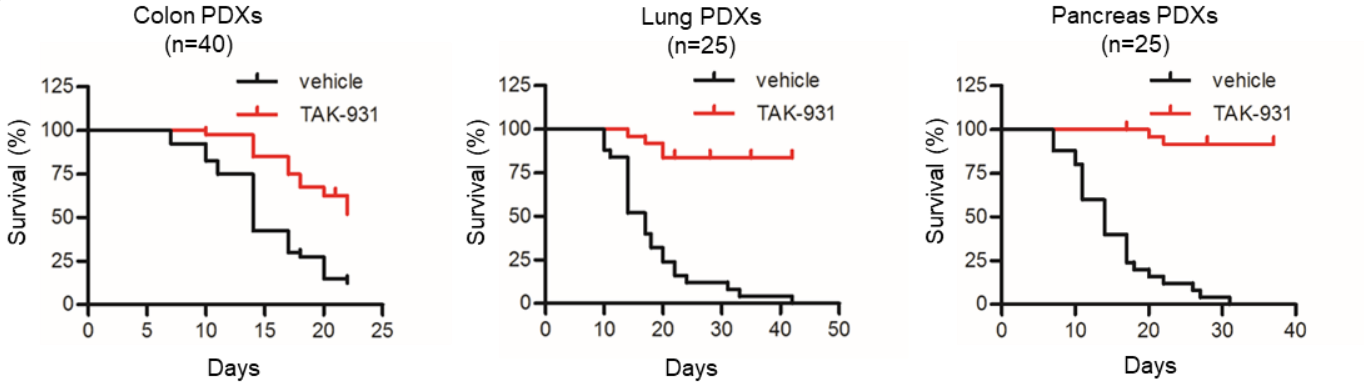

Fig. S7. Antitumor efficacy of TAK-931 in tumor xenograft mouse model. (A, B, C) Summary of %T/C and BWC in the COLO205 xenograft nude mouse model. COLO205-xenografted nude mice were orally administered TAK-931 at the indicated dose regimens, either continuously (A) or intermittently (B) (C) (n=5; day 15). (D) Antitumor efficacy of TAK-931 in the SW948 xenograft nude mouse model. SW948 xenografted nude mice were orally administered TAK-931 at the indicated dose regimens, either continuously (left) or intermittently (right). Efficacy data are plotted as mean tumor volumes (mm^3 ± SEM; n = 5). (E) Summary of %T/C and BWC on day 15. (F) Representative results of the efficacy study for sensitive (left) and resistant (right) PDXs. Black and red lines indicate vehicle and TAK-931 treatment, respectively. The efficacy data are plotted as mean tumor volumes (mm^3 ± SEM; n = 3). (G) Kaplan-Meier survival curve in 93 PDX models. Black and red lines indicate vehicle- and TAK-931-treated groups, respectively. Xenografted mice were orally administered TAK-931 at 60 mg/kg, twice daily, 3-days ON/4-days OFF, for the indicated cycles. Three mice were treated with vehicle or TAK-931 for each model.

A

GENESYMBOLS	Correlation
ARHGAP15	-0.30
CASR	0.35
DBF4	0.37
DCAF7	0.31
FBXO5	0.33
KDM4A	0.30
KIF5A	0.32
KRAS	0.30
NEUROD2	-0.30
NOTCH3	0.31
PVRL3	0.37
SEC13	0.30
SEC62	0.30
TCF7	0.30

B

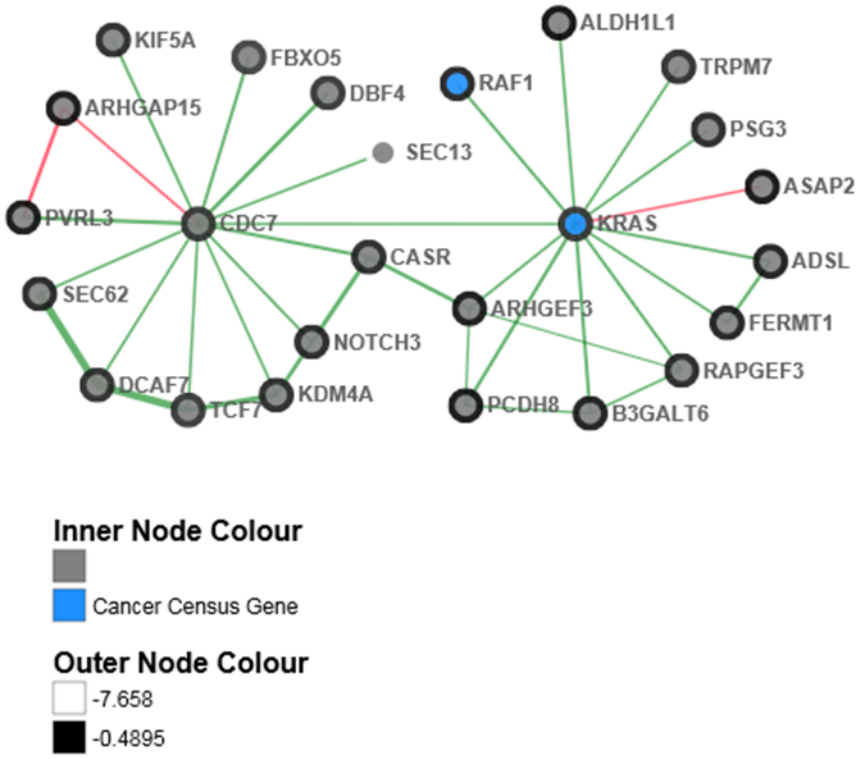

Fig. S8. Pathway network between CDC7 and KRAS knockdown. The network analysis of CDC7 and KRAS knockdown has been performed previously (*45*) <<https://oncologynibr.shinyapps.io/drive/>>. (A) The list of genes correlated with CDC7 knockdown effects is shown. The genes of which knockdown effects are correlated with CDC7 knockdown effects at > |0.3| are listed. (B) The pathway network of CDC7 and KRAS knockdown is shown. The network analysis was performed using CDC7 and KRAS as seed genes. The neighborhood correlations for CDC7 and KRAS are shown with positive correlations in green and negative correlations in red. The thickness of the lines between two genes represents the strength of the correlation.

Table S1. Phosphorylation sites modulated after 4 and 24 hours of TAK-931 treatment in COLO205 cells. Protein and gene names, ratios of phosphorylation changes, and amino acid positions are shown.

4 hours treatment				
Protein Names	**Gene Names**	**Ratio**	**Amino Acid**	**Positions**
MAX gene-associated protein	MGA	0.20	S	2712
Alpha-enolase	ENO	0.31	S	353
24 hours Treatment				
Protein Names	**Gene Names**	**Ratio**	**Amino Acid**	**Positions**
Cell division control protein 6 homolog	CDC6	2.34	S	45
Cell division control protein 6 homolog	CDC6	2.29	S	106
Fizzy-related protein homolog	FZR1	5.24	S	138
MAX gene-associated protein	MGA	0.21	S	2712
Nucleosome assembly protein 1-like 4	NAP1L4	0.27	S	12
Cell division cycle protein 20 homolog	CDC20	2.87	T	70
Cell division cycle protein 20 homolog	CDC20	3.48	S	41
Holliday junction recognition protein	HJURP	2.24	S	448
Inner centromere protein	INCENP	3.42	S	263
Inner centromere protein	INCENP	3.42	S	275
Kinesin-like protein KIF11	KIF11	2.43	T	926
Telomere-associated protein RIF1	RIF1	2.25	S	2196
Telomere-associated protein RIF1	RIF1	2.28	S	2172
DNA topoisomerase 2-alpha	TOP2A	2.69	S	1294
Rho GTPase-activating protein 11A	ARHGAP11A	2.64	S	585
ATPase family AAA domain-containing protein 5	ATAD5	2.35	S	44
Coiled-coil domain-containing protein 138	CCDC138	2.32	S	154
Cell division cycle-associated protein 2	CDCA2	2.38	S	936
CAP-Gly domain-containing linker protein 1	CLIP1	2.37	T	287
Disks large-associated protein 5	DLGAP5	2.71	S	618
Deoxynucleotidyltransferase terminal-interacting protein 2	DNTTIP2	2.54	S	434
Eukaryotic translation initiation factor 5B	EIF5B	2.64	S	1168
Band 4.1-like protein 1	EPB41L1	3.44	S	544;470
Band 4.1-like protein 1	EPB41L1	3.44	S	501
Band 4.1-like protein 1	EPB41L1	2.37	S	540;466
Band 4.1-like protein 1	EPB41L1	2.37	S	497
Eyes absent homolog 3	EYA3	2.33	T	269
Leucine-rich repeat-containing protein 16A	LRRC16A	2.57	T	1228
Antigen KI-67	MKI67	1.96	T	1261;901
Nucleolar and coiled-body phosphoprotein 1	NOLC1	0.31	T	620
Nucleolar and coiled-body phosphoprotein 1	NOLC1	0.31	T	617
Nuclear pore complex protein Nup214	NUP214	2.29	S	1963;1952;1953
DNA polymerase alpha subunit b	POLA2	2.54	S	141
E3 SUMO-protein ligase RanBP2	RANBP2	2.59	T	1412
E3 SUMO-protein ligase RanBP2	RANBP2	2.09	T	2613
E3 SUMO-protein ligase RanBP2	RANBP2	2.61	T	1178;2153;1177
Splicing factor, proline- and glutamine-rich	SFPQ	0.35	S	374
Shugoshin-like 1	SGOL1	2.33	S	256
C-Jun-amino-terminal kinase-interacting protein 4	SPAG9	2.42	S	183;183
C-Jun-amino-terminal kinase-interacting protein 4	SPAG9	2.51	S	245
Nucleoprotein TPR	TPR	2.32	S	1185
DNA repair protein XRCC1	XRCC1	2.40	S	226
DNA repair protein XRCC1	XRCC1	2.37	T	257
Uncharacterized protein C6orf132	C6orf132	2.21	T	661
Protein FAM83B	FAM83B	2.32	T	782
Histone H2B type 3-B	HIST3H2BB	0.44	S	39;39
Insulin receptor substrate 2	IRS2	0.25	S	1174
Uncharacterized protein KIAA1522	KIAA1522	4.97	S	400
PH and SEC7 domain-containing protein 3	PSD3	2.67	S	1012
Supervillin	SVIL;SVIL	2.50	S	694

Table S2. %T/C values of antitumor efficacy studies in colorectal, lung, ovarian, and pancreatic PDXs.

Model ID	Tumor Type	TGI (%)	TGI endpoint (Day)	BWC (%)
CR_1	Colon	80.0	22	-7.1
CR_2	Colon	97.6	21	-8.7
CR_3	Colon	89.3	22	-3.5
CR_4	Colon	66.4	22	-12.3
CR_5	Colon	85.6	22	-9.1
CR_6	Colon	79.7	22	-11.7
CR_7	Colon	70.8	22	-5.0
CR_8	Colon	64.0	22	-18.6
CR_9	Colon	59.7	22	-14.3
CR_10	Colon	48.4	22	-9.5
CR_11	Colon	53.5	22	-4.7
CR_12	Colon	54.6	22	-11.9
CR_13	Colon	38.7	22	-6.4
CR_14	Colon	48.3	22	-0.1
CR_15	Colon	54.5	22	-6.7
CR_16	Colon	50.2	22	-7.2
CR_17	Colon	54.6	22	-15.4
CR_18	Colon	50.1	22	-13.9
CR_19	Colon	51.1	22	-15.0
CR_20	Colon	38.6	22	-9.2
CR_21	Colon	45.1	22	-13.9
CR_22	Colon	35.4	22	-10.9
CR_23	Colon	49.5	22	-15.4
CR_24	Colon	41.6	22	-7.8
CR_25	Colon	42.3	22	-5.2
CR_26	Colon	42.5	22	-3.7
CR_27	Colon	38.3	22	-6.3
CR_28	Colon	38.7	22	-8.5
CR_29	Colon	36.1	22	-5.1
CR_30	Colon	33.9	22	-11.9
CR_31	Colon	35.2	22	-14.5
CR_32	Colon	28.4	22	0.4
CR_33	Colon	17.1	22	-6.6
CR_34	Colon	21.9	22	-1.1
CR_35	Colon	15.7	22	-5.9
CR_36	Colon	18.6	22	-12.8
CR_37	Colon	15.3	22	-11.9
CR_38	Colon	10.2	22	-3.9
CR_39	Colon	3.8	22	-18.6
CR_40	Colon	2.9	22	-13.3
LU_1	Lung	82.8	22	-11.6
LU_2	Lung	70.0	22	-9.2
LU_3	Lung	43.9	22	0.0
LU_4	Lung	21.5	22	-10.4
LU_5	Lung	94.4	35	-10.2
LU_6	Lung	90.2	22	-5.9
LU_7	Lung	91.4	22	-4.8

Model ID	Tumor Type	TGI (%)	TGI endpoint (Day)	BWC (%)
LU_8	Lung	84.7	33	-6.9
LU_9	Lung	81.9	42	-5.1
LU_10	Lung	99.1	22	-6.4
LU_11	Lung	97.8	17	-8.2
LU_12	Lung	95.4	22	-8.5
LU_13	Lung	79.8	26	-9.2
LU_14	Lung	78.9	22	-8.0
LU_15	Lung	78.1	22	-5.9
LU_16	Lung	72.4	22	-9.0
LU_17	Lung	73.3	22	-7.0
LU_18	Lung	76.8	20	-4.5
LU_19	Lung	67.9	22	-2.8
LU_20	Lung	54.0	22	-3.1
LU_21	Lung	59.0	22	-5.8
LU_22	Lung	53.1	22	-6.9
LU_23	Lung	55.3	22	-4.3
LU_24	Lung	50.8	22	-6.9
LU_25	Lung	30.8	22	-3.7
OV_1	Ovary	71.7	22	-7.3
OV_2	Ovary	57.4	22	-4.2
OV_3	Ovary	56.5	22	-14.9
PA_1	Pancreas	98.5	22	-6.0
PA_2	Pancreas	82.6	22	-6.8
PA_3	Pancreas	84.2	22	-17.5
PA_4	Pancreas	73.0	22	-5.3
PA_5	Pancreas	66.2	22	-4.1
PA_6	Pancreas	66.5	22	-12.5
PA_7	Pancreas	54.0	22	-8.2
PA_8	Pancreas	56.5	22	-6.5
PA_9	Pancreas	52.2	22	-15.3
PA_10	Pancreas	41.7	22	-17.4
PA_11	Pancreas	23.8	22	-9.5
PA_12	Pancreas	85.8	22	-15.5
PA_13	Pancreas	89.0	22	-8.0
PA_14	Pancreas	79.2	28	-2.4
PA_15	Pancreas	81.7	22	-2.0
PA_16	Pancreas	86.7	22	-8.1
PA_17	Pancreas	81.3	22	-5.8
PA_18	Pancreas	73.3	22	-5.4
PA_19	Pancreas	64.6	37	-1.8
PA_20	Pancreas	54.6	28	-6.3
PA_21	Pancreas	67.7	22	-6.6
PA_22	Pancreas	73.3	17	-5.7
PA_23	Pancreas	70.1	22	-4.7
PA_24	Pancreas	55.1	22	-3.1
PA_25	Pancreas	40.5	22	-10.8